Extending the glass formation of alkali tellurites

Yi Wei, ^a Aaron Philips, ^a Nils Empen, ^a Brittany Thompson, ^b Lisa Tarman, ^c Ethan Frana, ^a Lauren Meyer, ^a Caio Bragatto ^a & Steve Feller ^{a,1}

Manuscript received 23 March 2023 Revision received 12 October 2023 Manuscript accepted 12 November 2023

The physical properties of low alkali content tellurite glasses of composition $xM_2O.(1-x)TeO_2$ ($0 \le x \le 0.35$) have been previously collected in this laboratory. The twin-roller rapid quenching technique (cooling rate> 10^5 °C/s), used within a nitrogen environment, successfully and significantly extended the glass-forming range in the lithium and sodium tellurite systems. The upper range for modification has been extended from x=0.35 to 0.80 and up to x=0.625 for the lithium and sodium systems, respectively. In the K, Rb and Cs tellurites, the glass forming ranges were not increased. Glass transition temperature (T_x), crystallisation temperature (T_x), density, molar volume, packing fraction, ionic conductivity and Raman spectra were obtained for these glasses. These results showed structural changes as a function of composition and carbonate retention in the glasses as the amount of alkali modifier increased above x=0.5.

1. Introduction

Recently, glassy tellurium dioxide and TeO₂-based glasses have received considerable attention and many studies have been done to investigate their properties. (1-10) Nonlinear optical susceptibilities of $x(M_2O).(1-x)TeO_2$ with M=Li, Na and K were measured by Kim. (1) The ionic conductivity of binary alkali tellurite glasses was tested by Nascimento's group. (2) The thermal behaviour of Na₂O-TeO₂ glass was measured by Kavaklıoğlu's group. (3) Kavaklıoğlu further mentions that sodium tellurite glasses were made up to x=0.465. Much research on the structure and spectroscopy has been done on these glasses, including Raman studies of $x(MO_{1/2}).(1-x)TeO_2$ with M=Li, Na, K, Rb, Cs, and Ti by Sekiya⁽⁴⁾ and neutron diffraction studies of M=Li, Na and K done by Barney. (5) Two-dimensional NMR spectroscopy by Sen et al⁽⁶⁾ was performed on pure TeO₂ glass. Both ¹⁷O and ¹²⁵Te NMR were done by Joseph Zwanziger's group on a sample of glassy TeO_2 enriched in $^{17}\text{O.}^{(7)}$ Several groups secured data and analysis by neutron scattering and XRD^(8,9) on glassy TeO₂ and alkali tellurite glass. Thermal properties, density and structure analysis by XRD and Raman data of tellurium and zinc tellurite glasses were determined by Kamitsos' group. (10) Also, thermal properties and Raman spectra were obtained from low-modified alkali tellurite glass ($x \le 0.30$) by the present group.⁽¹¹⁾

However, in all reported studies, there is a lack of data about highly modified alkali tellurite glasses. By em-

ploying the twin-roller quenching technique in a nitrogen glove box, we were able to form $x(M_2O).(1-x)TeO_2$ glasses with M=Li, Na in the range of $0.00 \le x \le 0.8$ for Li and $0.00 \le x \le 0.625$ for Na. Glass in the K, Rb and Cs tellurites were made up to x=0.35. In the present study, property and structure data were compared with the literature's thermal properties, density, ionic conductivities and Raman spectra. A comparison of structure and property was performed as well. This is the first report of very high alkali content tellurite glasses.

2. Experimental procedures

2.1. Glassmaking

Alkali carbonates, and tellurium dioxide were measured into a platinum crucible and then stirred for 5 min to ensure that the two components were completely mixed. Afterward, the samples were heated and melted in an electric furnace at 1000°C for lithium up to x=0.25 and sodium up to x=0.20. All other samples were melted at 850°C with the temperature adjusted to minimise the loss of starting material. Some of the highly modified glasses were heated in a nitrogen glove box to prevent the sample from being attacked by water in the air. After 15 min, samples were removed, cooled and weighed to ensure the accuracy of the glass composition. To quench the glass, the material was put back into the furnace and reheated for 10 min at the same temperature as the first heating. The lowest modified glasses $(0 \le x \le 0.15)$ were swirled in the crucible and then the crucible bottom was dipped into cold water. (10)

 $^{1}\textsc{Corresponding}$ author. Email: SFELLER@coe.edu DOI: 10.13036/17533562.65.1.07

^a Coe College Department of Physics, Cedar Rapids, IA 52402, USA

^b Northeast Community College, Lincoln, NE 68701, USA

^c William Penn High School, York, PA 17403, USA

Glasses between $0.15 \le x \le 0.35$ were plate quenched, and the higher modified glasses were roller quenched to obtain glassy samples. All glass samples made were clear.

2.2. Carbonate retention

Usually in glass-making, it is supposed that all the CO_2 in a carbonate ingredient is lost on melting, e.g. $Na_2CO_3 \rightarrow Na_2O$ (melt) + CO_2 (gas). However, for high modifier content, there is evidence that a fraction of the CO_2 is retained in the melt and glass. (12)

The fraction of carbon dioxide retention (R_{CO_2}) was calculated using the predicted mass loss (M_{predict}) and the actual mass difference (M_{diff}). We used the following equations:

$$M_{\text{diff}} = M_{\text{predict}} - M_{\text{actual}}$$
 (1)

$$R_{\text{CO}_2} = M_{\text{diff}} / M_{\text{predict}}$$
 (2)

where M_{actual} is the experimental mass loss and M_{predict} is the predicted mass of the byproduct CO_2 (as determined by the starting glass chemical equation.). Note that since the sample is volatile, Equation (2) underestimates the retention of carbonate.

The effects of carbonate retention is to lower the modification levels above a batch x=0·5 in both the sodium and lithium systems. After accounting for carbonate retention the modifications became on average: x=0·54 for lithium tellurites and x=0·52 for sodium tellurites. This and unpublished Raman results that indicate the sodium tellurite glass and crystal have the same modification at x=0·5 gives us confidence that the net modification is lowered by a relatively small and predictable amount except, possibly, the highest modified lithium and sodium glass.

Raman spectra of the higher sodium content glasses shown here are consistent with the slowly varying glass compositions consistent with the carbonate retention as reported in the paper.

2.3. Thermal measurements

A Q200 TA Differential Scanning Calorimeter (DSC) was employed to determine the thermal properties for temperatures ≤400°C. Approximately 60–90 mg of each sample were measured into a small aluminium pan with a lid. The pan was then put into the DSC. A heating rate of 40°C/min, over the range of 40–400°C, was used under flowing nitrogen gas for each measurement. An indium standard was periodically used to check the calibration. A Perkin-Elmer STA 6000 Simultaneous Thermal Analyser with alumina sample cups was used for glasses with higher transition temperatures. Indium and zinc were used as reference materials. Approximately 30–60 mg of sample was used for this analysis. A heating rate of 40°C/min, from

50–1000°C under gaseous nitrogen, was used for each measurement. The glass transition temperature ($T_{\rm g}$) was found by the onset inflection of the endothermic glass transition event, and the onset of the inflection point of the subsequent exothermic event determined the first crystallisation temperature ($T_{\rm x}$). The glass's thermal stability, or it's crystallisation resistance (ΔT), was calculated with the equation:

$$\Delta T = T_x - T_g \tag{3}$$

2.4. Raman spectroscopy

Raman spectroscopy was conducted to identify the atomic-level structure of these glasses. The samples were measured in a Jasco NRS-3100 Laser Raman Spectrophotometer. Each sample was examined before it was measured to make sure it was visibly clear and glassy. Each sample was exposed to a 784-68 nm laser for 10 to 30 s twice, with the intensity and time adjusted to prevent crystallisation and damage to the sample. The spectra were taken over the wavenumber range from 150–1900 cm⁻¹.

2.5. Density measurements, molar volumes, packing fraction

Two pycnometers, an Ultrapycnometer 1000 and a Micropycnometer both from Quantachrome Corporation, were used to determine volume en route to the density (ρ) of the glasses. The pycnometers operated at approximately 24°C using helium gas. Three measurements were taken, each with fifteen runs. The first measurement taken was with aluminium of the same volume as the sample, then the sample, and then a final measurement of the aluminium. The average of the last five sample densities was adjusted by the variation in the measured density values of aluminium to its known value of 2·70 g/cm³, as found by NIST. (13) Before and after aluminium runs were to ensure that any temperature drift was accounted for. Densities from samples that were roller-quenched are not feasible using thin flakes due to the large volumes required for the pycnometer. Our usual method for roller-quenched samples, the sink-float method, is not possible due to its limited upper density of 3.32 g/cm³.

The molar volume of the glass, *mv*, was calculated with the following equation using the density found by pycnometry:

$$mv = (xMM_{M_2O} + (1-x)(MM_{TeO_2}))/\rho,$$
 (4)

where MM is the value for the molar masses and x is the molar fraction of modifier oxide. Through calculating the volumes of the constituent atoms in a mole of glass using Equation (5)

Volume of the atoms in a mole= $(\Sigma(4/3)\pi(R_i)^3)*N_A$ (5)

where R_i is the Shannon radii of the ith ions in the

glass^(14,15) and N_A indicates Avogadro's number. The radii, adjusted for coordination, used in this paper are shown in Table 1.

The packing fraction, *pf*, was calculated by: *pf=volume of the atoms in a mole/mv* (6)

2.6. Ionic conductivity

Roller-quenched samples were further prepared into electrodes using a stainless steel mould and aluminium foil; the sample preparation procedure is described elsewhere. Then, samples were placed in a homemade tube furnace and sample holder, and electrical impedance spectroscopy (EIS) measurements were made at different temperatures using a Gamry Interface 1010T Potentiostat. To determine the ionic conductivity of the samples, EIS data were analysed by fitting an equivalent electrical circuit model Using software provided by Gamry (Echem Analyst). By determining the resistance (R) of the glassy phase, the ionic conductivity (σ) was calculated by:

$$\sigma = (1/R)(l/A) \tag{7}$$

where l and A are the thickness and the cross-sectional area of the electrode-part of the pellet, respectively. The data collected were plotted as $\log(\sigma T)$ as a function of 1000/T to determine the activation energy of the process. Since the ionic conductivity is considered an activated process, the slope of such a plot is proportional to the activation energy according to

$$\log(\sigma T) = \log \sigma_0 - E_A / (k_B T) \tag{8}$$

where σ_0 is the pre-exponential term, E_A is the activation energy of the process, and k_B is Boltzmann's constant.

3. Results and discussion

3.1. Experimental results

The physical properties of the alkali tellurite glasses are listed in Table 2.

3.2. Glass forming ranges

Lithium tellurite glasses were made successfully over the range of $0 \le x \le 0.40$ and $0.60 \le x \le 0.80$. The samples were heated, and plate-quenched in air when $x \le 0.35$ to form glasses. For x > 0.35 and after the second heating at 850°C in the nitrogen glove box and roller quenching, a combination of glass and crystal formed for x = 0.40, 0.60, 0.65, 0.70, 0.78, and 0.80. Enough sample for thermal measurements was present in

Table 1. Ionic radii used in the packing fraction^(14,15)

the form of flakes of glass The x=0.50 composition was attempted using the same method, but it fully crystallised.

Sodium tellurite glass was formed over the range of $0 \le x \le 0.65$. Samples were able to be made into glass in air using plate quenching when $0 \le x \le 0.35$. For x > 0.35, samples required roller quenching to form glass. For $x \ge 0.45$ glass, the process changed to roller quenching in a glove box in order to prevent atmospheric water attack and to preserve the sample as an amorphous solid. For these materials, only a very small amount of glass was present, even when the process was carried out in a glove box and using the roller quenching technique. However, the flakes were large enough to perform thermal measurements

Potassium tellurite glass was made successfully from $0 \le x \le 0.35$. For $x \le 0.25$ glass was made in-room air conditions by plate quenching, and the x = 0.35 glass was made via roller quenching. Glass formation was attempted for $0.40 \le x \le 0.65$, but the samples crystallized when made in the glove box.

Rubidium tellurite samples were made into glass from $0 \le x \le 0.35$. The material formed into glass in room air directly when $x \le 0.25$. When x = 0.30, the glass was made with an intermittent quenching technique. The intermittent quenching method was carried out by melting and coating the bottom of a platinum crucible with a thin layer of sample. The crucible was then dipped into a mixture of ice and water, being careful to not let water enter the crucible. The x = 0.35 composition was made into glass after roller quenching in the glove box. The x = 0.60 was attempted in the glove box, but it crystallised after quenching.

Cesium tellurite glass was made in the region $0 \le x \le 0.25$. Samples were made in the glove box with the roller quench method and came out partly crystallised at every composition. It should be noted that the amount of crystallisation visibly increased as more modifier was added.

3.3. Thermal properties

Glass transition temperatures for alkali tellurite glasses are shown in Table 2 and Figure 1.

The glass transition temperature of lithium tellurite glass are shown in Figure 1 (blue). The glass transition temperature generally decreased over the glass forming range. This is thought to be due to the ionic Li–O bond (150 kJ/mol),⁽¹⁸⁾ which has less energy than the Te–O covalent bond (285 kJ/mol).⁽¹⁰⁾ The glass transition temperature for sodium tellurite generally decreases over the glass forming range due to the strength of the Na–O bond (84 kJ/mol) being less than the Te–O covalent bond (285 kJ/mol),⁽¹⁰⁾ Figure 1 (red). Due to the Na–O bond being weaker than the Li–O bound, the $T_{\rm g}$ of sodium tellurite is lower than lithium tellurite.

YI WEI ET AL: EXTENDING THE GLASS FORMATION OF ALKALI TELLURITES

Table 2. The physical properties of the alkali tellurite glasses

	Molar fraction (x)	T_g (°C) ±4°C	T_x (°C) ±4°C	ΔT (°C) ±6°C	ρ (g/cc) ±1%	Molar volume (cm3/mol) ±1%	Packing fraction	Activation energy for ionic conductivity (eV)
Li	0	305	348	43	5.57	28.7	0.357	
	0.05	293	347	54	5.45	28.1	0.357	
	0.1	282	352	70	5.30	27.7	0.356	
	0.15	270	348	78	5.19	27.0	0.358	
	0.2	263	368	105	5.01	26.7	0.355	1.195
	0.25	254	336	82	4.80	26.5	0.350	
	0.25	256			4.82	26.4	0.352	
	0.3	250	200	(0	1.71	26.2	0.247	0.742
	0.3	248	308	60	4.61	26.2	0.347	0-742
	0.35	243	298	55	4.41	25.9	0.344	0.702
	0.4	244	289	45				0.703
	0.6	256	277	21				0.625
	0.625	252	278 274	26				
	0·65 0·7	244 233	259	30 26				0.618
	0.75	224	241	17				
	0.8	212	222	10				
	0.8	214	225	11				
Na	0	305	348	43	5.57	28.7	0.357	
ING	0.05	296	335	39	5.41	28.6	0.361	
	0.1	282	366	84	5.25	28.5	0.366	
	0.15	268	472	204	5.06	28.7	0.368	
	0.15				5.00	29.0	0.364	
	0.2	252			4.88	28.7	0.371	
	0.2	256	443	187	4.89	28.7	0.371	
	0.2							0.706
	0.25	240			4.67	28.9	0.372	
	0.25	240	372	131	4.58	29.5	0.365	
	0.3		312		4.46	29.2	0.372	
	0.3							0.69
	0.35	222	303	81	4.24	29.6	0.371	
	0.4	217	247	30	4.03	29.9	0.370	
	0.4							0.719
	0.45		220		3.79	30.5	0.367	
	0.5	232						
	0.575		228					
	0.58	224	228	4				
	0.6	212	226	13				
	0.6	215	226	11				
	0.625 0.625	210 210	222 222	12 12				
K	0.623	305	348	43	5.57	28.7	0.357	
IX	0.05	297	370	73	5.30	29.5	0.375	
	0.1	282	376	94	5.05	30.3	0.393	
	0.15	262	416	154	4.78	31.4	0.407	
	0.2	240	326	86	4.55	32.2	0.423	
	0.25	221			4.32	33.1	0.436	
	0.25	221	305	84				
	0.3	205						
	0.3	208	255	47				
	0.35	185	202	18				
	0.35		200					
	0.6		222					
Rb	0	305	348	43	5.57	28.7	0.357	
	0.05	299			5.35	30.1	0.377	
	0.1	280			5.16	31.5	0.395	
	0.1				5.18	31.3	0.398	
	0.15	256			5·01	32·7	0.415	
	0.15	256			5.01	32·7	0.415	
	0·2 0·2	233	297	64	4·88 4·86	33.9 33.9	0·433 0·432	
	0.2	233	<u> </u>	04	4·86 4·83	34·2	0.432	
	0.25	250			4.83	34.4	0.458	
	0.25	212	273	62	4.73	35.2	0.438	
	0.25	204	210	02	4.67	35.6	0.475	
	0.23	191	242	51	107	55 5	0 1/0	
	0.3	201	-74	91	4.57	36.8	0.490	
	0.35	122			10,	200	0 270	
Cs	0	305			5.57	28.7	0.357	
	0.05	296			5.41	30.6	0.386	
	0.1	274			5.28	32.6	0.411	
	0.15	244			5.10	34.9	0.429	
	0.2				5.11	36.0	0.416	

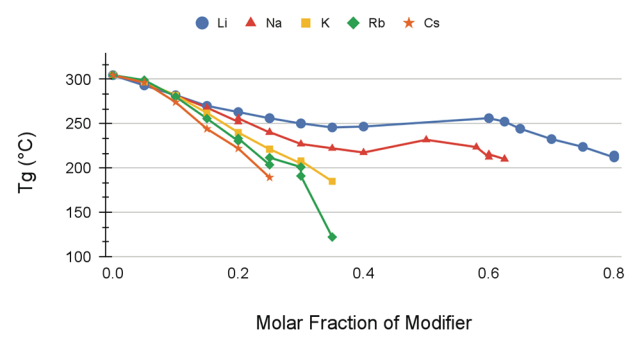


Figure 1. The glass transition temperatures of the alkali tellurite glass system. The error bars are smaller than the data points [Colour available online]

The results for the sodium tellurite $T_{\rm g}$ are compared in Figure 2 with Kavaklıoğlu's results over the range $0.075 \le x \le 0.40$. We can see there is a consistent trend between the two sets of measurements. The main difference between the two results is that in the results from Istanbul Technical University, the $T_{\rm g}$ slightly increased between x=0.33 and 0.40. However, in the present study, the increasing trend began at x=0.40.

The potassium tellurites (Figure 1, yellow), rubidium tellurites (Figure 1, orange), and cesium tellurites (Figure 1, green) have a decreasing trend in glass transition temperature as *x* increases between 0 and 0·35. This, again, is due to the significant difference in strength between the M–O ionic bond (M=K, and Rb). and the Te–O covalent bond. For potassium, the difference is 231 kJ/mol and for rubidium, the difference is 235 kJ/mol.

The crystallisation temperatures of the alkali tellurites are displayed in Figure 3 while Figure 4 depicts the stability temperature range ($=T_x-T_g$). This latter figure shows that the most stable glass compositions occur near x=0.2 for all alkali tellurites. Sodium is the most stable of the alkali systems.

3.4. Density

Figures 5–7 display the densities, molar volumes, and packing fractions of the alkali tellurite glasses.

Due to the increase in modifier content and the

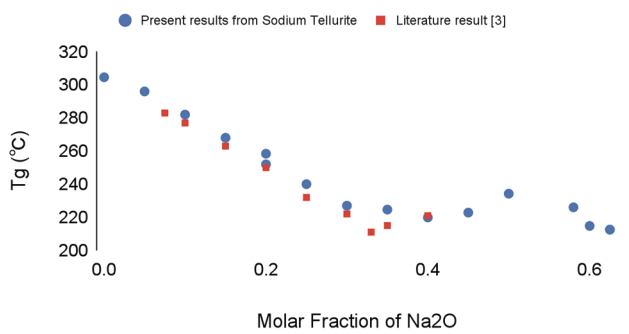


Figure 2. The glass transition temperatures of the Na_2O-TeO_2 system compared with results from Kavaklıoğlu et al.⁽³⁾ The error bars are smaller than the data points [Colour available online]

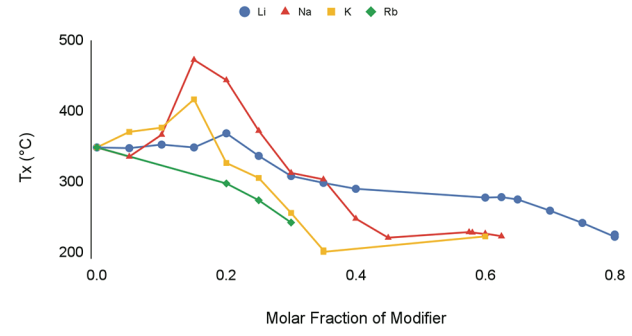


Figure 3. The crystallisation temperatures of the alkali tellurite system as a function of molar percentage modifier. The experimental error bars are smaller than the data points [Colour available online]

fact that lithium oxide has a lower density compared to tellurium dioxide, the density of lithium tellurite glasses decreases from 5.57 to 4.41 g/cm³ over the range $0 \le x \le 0.35$; This is shown in Figure 5 (blue). The molar volume and packing fraction were also calculated, and are shown sequentially in Figures 6 (blue) and 7 (blue). Since the radius of a lithium ion is less than that of oxygen, the lithium ions can fill in the gaps between oxygens. Therefore, the molar volume of lithium tellurite glass decreases as the modifier content increases. The oxygen content controls the packing fraction and is flat when x < 0.15, and then decreases until x = 0.35.

Sodium tellurite glass has a decreasing density from 5·57 to 3·79 g/cm³ over $0 \le x \le 0.45$, which is shown in Figure 5 (red). The radii of sodium ions are smaller than the radii of oxygens (the difference is less than 15%), and the packing fraction (Figure 7, red) slightly increases over $0 \le x \le 0.20$. It then slightly decreases from x=0.20 to 0.45. However, the sodium ion starts to fill in the gaps and 'substitute' for the volume of missing oxygen, therefore the molar volume has no significant change over the glass forming range which is shown in Figure 6 (red).

The density of potassium tellurite glass (Figure 5, yellow) decreases from 5.57 to 4.43 g/cm³ from x=0 to 0.25. Over the range $0 \le x \le 0.45$ for rubidium tellurite glass (Figure 5, green), the density decreases from 5.57 to 4.57g/cm³. Cesium tellurite glass density (Fig-

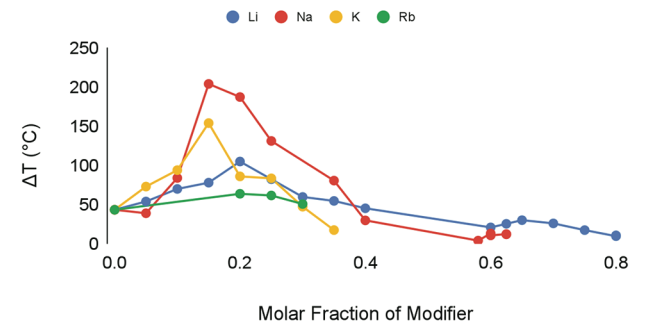


Figure 4. The stability of the alkali tellurite system. The error bars are smaller than the data points [Colour available online]

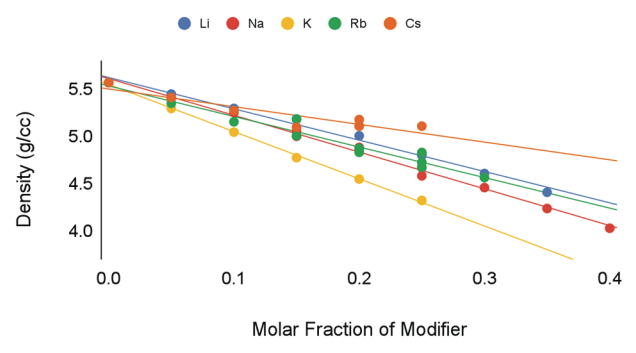


Figure 5. The density of the alkali tellurite glass system. The lines are guides to the eye. The error bars are smaller than the data points [Colour available online]

ure 5, orange) increases from 5.57 to 5.72 g/cm³ over the range of $0 \le x \le 0.20$. Due to the radii of these three alkali ions being larger than the radii of oxygens, the modifier ion expands the molar volume (Figure 6), and packing fractions (Figure 7) increase with the increase of modifier content.

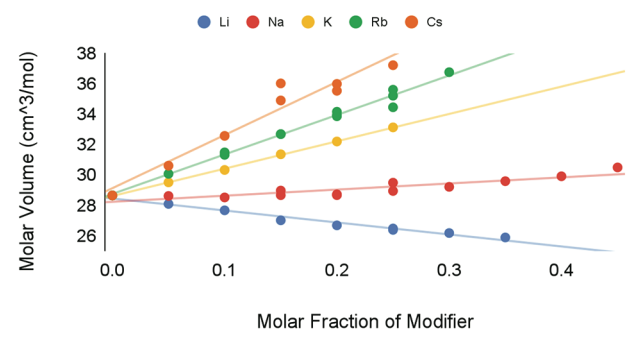


Figure 6. The molar volumes of the alkali tellurite glass system The lines are guides to the eye. The error bars are smaller than the data points [Colour available online]

4. Raman spectroscopy results

Representative Raman spectra of alkali tellurite glasses are shown in the following section.

Figure 8 shows the Raman spectra of the lithium tellurite glasses. In each spectrum, several peaks were observed. One peak is in the wave number region

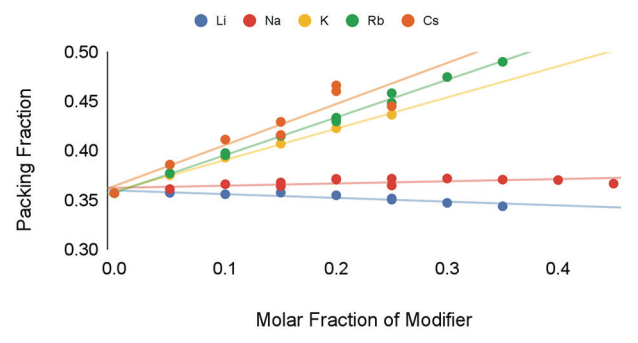


Figure 7. The packing fraction of each alkali tellurite glass system. The lines are guides to the eye. The error bars are smaller than the data points [Colour available online]

760–780 cm⁻¹, where it is growing in intensity with increasing amounts of the modifier. There is another peak in the region 670–680 cm⁻¹. The intensity seems to be level or close to it as composition changed. The last peak is over the region between 450–460 cm⁻¹. This feature decreases and has the lowest intensity at x=0·40. These peaks are similar to those found in zinc tellurites as found by Tagiara. (19,20)

The Raman spectra of sodium tellurite glasses, shown in Figure 9, were obtained over the region $0.15 \le x \le 0.40$. Three peaks were observed and distributed sequentially in wavenumber regions 785–795, 660–680 and 460–470 cm⁻¹. The intensity of the peak in region 785–795 cm⁻¹ grows as the modifier content increases, and at the same time, the peaks around 660–680 and 460–470 cm⁻¹ are decreasing slowly or remaining fairly constant.

In the Raman spectra of potassium tellurite that were measured at x=0.25, 0.30, and 0.35 (Figure 10), three peaks were observed in the wave number regions 770–785, 655–665 and 470–480 cm⁻¹. The peak at region 770–785 cm⁻¹ increases and the rest of the peaks decrease or remain fairly constant as modifier content increases from x=0.25 to 0.35.

The rubidium tellurite Raman spectra are shown in Figure 11. Three peaks were observed in the regions of wave numbers 770–780, 650–670, and 440–460 cm⁻¹. The peak near 770–780 cm⁻¹ increases as the modifier

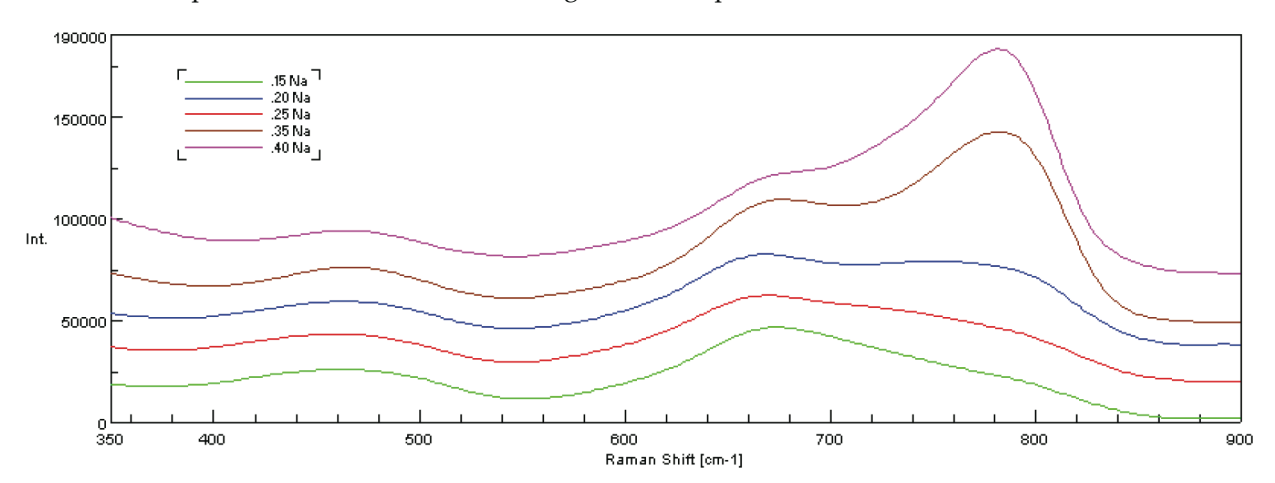


Figure 8. Raman spectra for $xLi_2O^*(1-x)TeO_2$ (x=0.25, 0.3, and 0.4). A vertical offset was used [Colour available online]

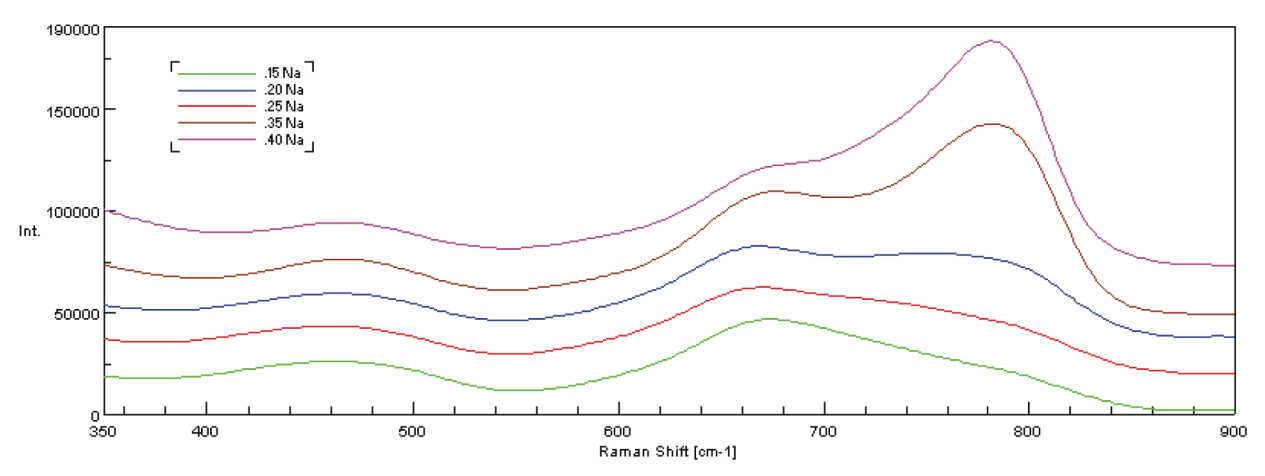


Figure 9. Shows the Raman spectra for $xNa_2O^*(1-x)TeO_2$ (0·15 $\le x \le 0$ ·65). A vertical offset was used [Colour available online]

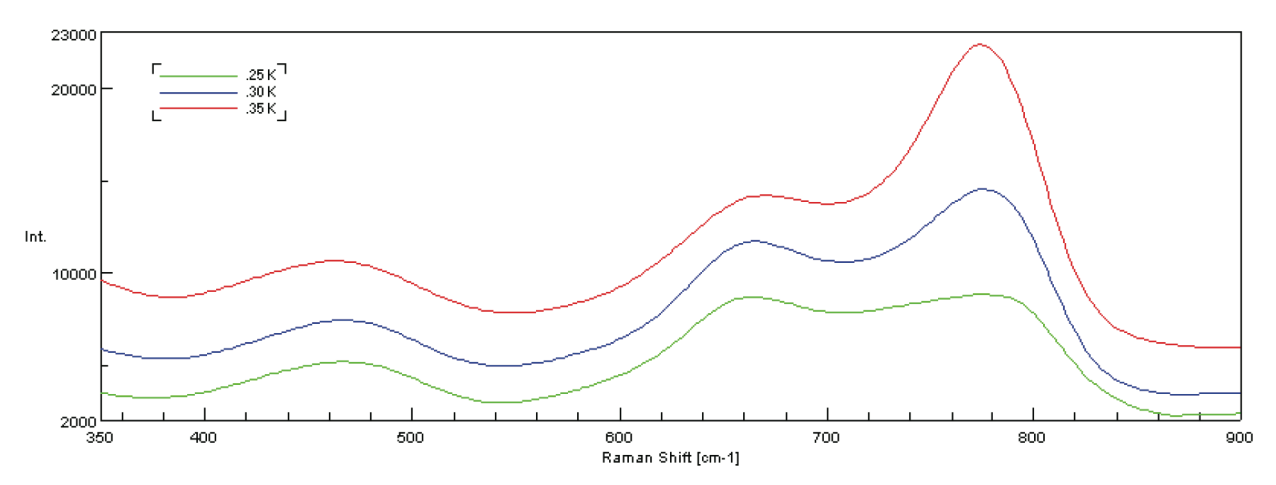


Figure 10. Raman spectra for $xK_2O^*(1-x)TeO_2$ (x=0.25, 0.30, 0.35). A vertical offset was used [Colour available online]

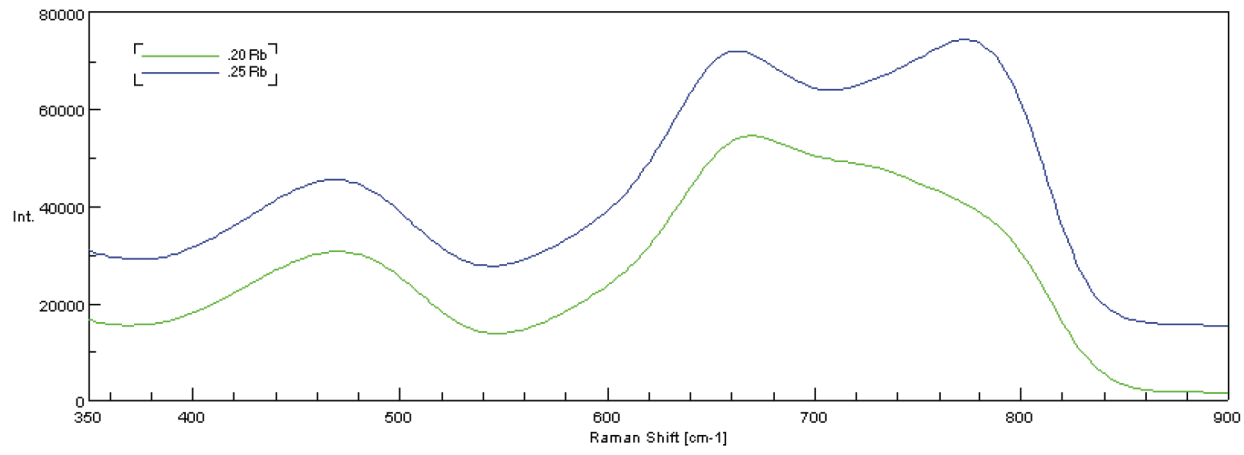


Figure 11. Shows the Raman spectra for $xRb_2O^*(1-x)TeO_2(x=0.20, 0.25)$ A vertical offset was used [Colour available online]

percentage increases. Due to the highly hygroscopic characteristic of rubidium tellurite glass, the Raman spectra could not be measured for higher modifier content glass.

There are three Raman peaks around 770, 660, and 460 cm⁻¹, all of which are very consistent among the studied compositions. (19,20) The peak above 700 cm⁻¹ indicates the asymmetric stretching of Te–O–Te

bridges that connect TeO₄ trigonal bipyramids (tbp) with TeO₃ species.⁽¹⁹⁾ The peak around 670 cm⁻¹ presents the in-phase symmetry stretching/breathing vibration of double Te–O₂–Te bridges,^(19,20) and the third peak at 460 cm⁻¹ indicates the M–O–Te bond's vibration (where M is presenting as modifier), which substitutes the Te–O–Te bond.^(19,20) The trend of the increased amount of three-coordinate tellurite in the

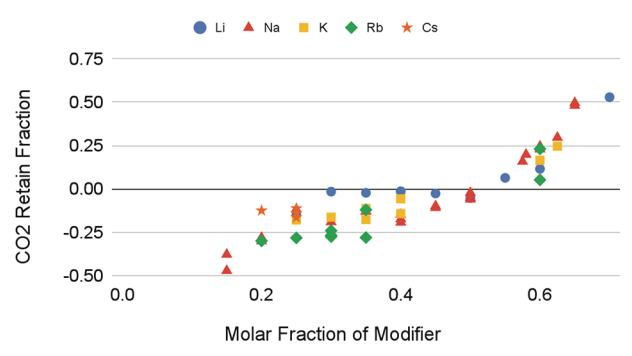


Figure 12. The fraction of carbonate retained in the alkali tellurite system. Fractions <0 mean that the experimental weight loss is more than predicted, and fractions >0 mean that the weight loss was less than the predicted weight loss [Colour available online]

structure is presented by the rise of the 770 cm⁻¹ peak with the increase of modifier content.^(19,20)

The comparison of zinc tellurites to the alkali tellurites shows similar peaks which we interpret to mean similar structures are present.

5. Carbonate retention

Carbonate retention occurred in the sample when x>0.50. This was observed by comparing the actual weight loss ($M_{\rm actual}$) with the predicted weight loss ($M_{\rm predict}$), see Equations (1) and (2). We concluded that carbonate was retained when $M_{\rm actual}$ was less than $M_{\rm predict}$. The fraction of carbonate retention was calculated using Equation (2) and found when x>0.50, which is shown in Figure 12. Here, negative retention means that excessive weight was lost in the

heating of the sample, and positive retention means that carbonate was retained in the heating of the sample (with the proviso that some of the sample was lost to volatilisation). In the spectra of alkali tellurite glass, the vibration of carbonate species is present in the glass in the range of 1050–1070 cm⁻¹. This peak shows up when x>0.50, and it corresponds with the weight loss measurements shown in Figure 12. Raman peaks in the same wavenumber region from highly modified borates have been reported by Kamitsos' group and it is from the symmetric stretch of the $(CO_3)^{-2}$ group. (12) The lithium tellurite T_g s show a change in trend past 50 molar percent lithia. This is the region where carbonate retention commences. The structural origin on T_{σ} is not known but the trend is similar to that found in borates and borosilicates. (21)

6. Ionic conductivity

Nyquist plots for the lithium containing tellurite glasses were taken at different temperatures for each sample. In these plots, they presented one half-circle followed by an infinite impedance, as expected for a sample with a single phase, up to *x*=0·65. An example of these plots collected at different temperatures can be seen in Figure 14. For each of the glass compositions measured, data were collected at different temperatures in order to graph an Arrhenius plot. See Figures 15 and 16 for glassy lithium and sodium tellurites, respectively.

For these data, curves were fit using OriginPro 8.5 software and had a minimum R^2 of 0.95 (R^2 is the coefficient of determination, used to determine how

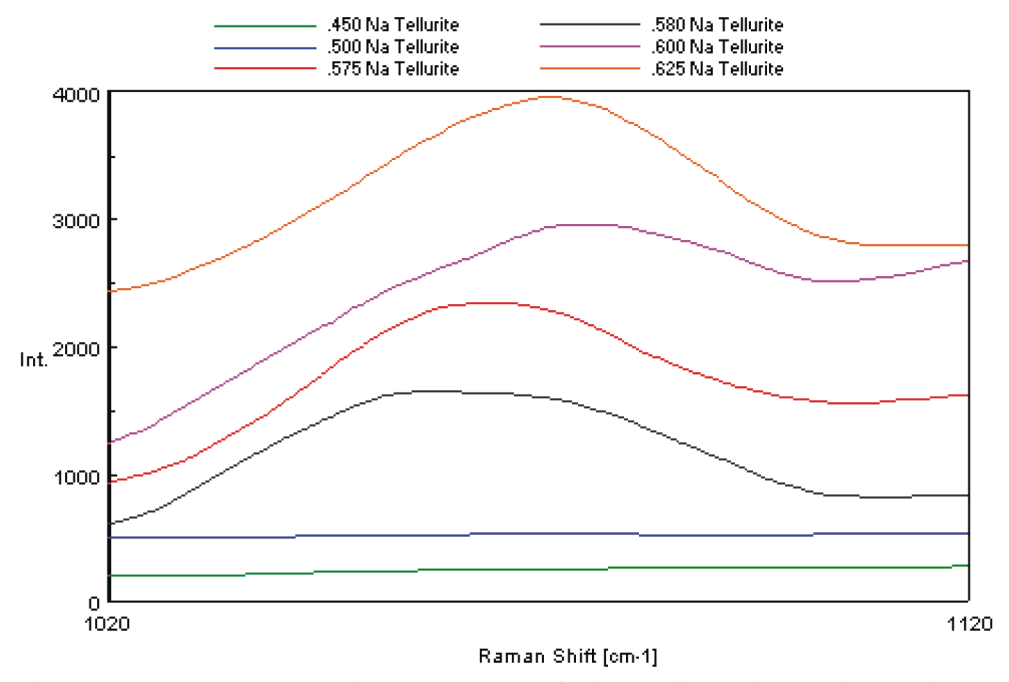


Figure 13. Carbonate retention is present in the Raman spectra of sodium tellurite glasses. Their peaks maximize over the approximate range $1050-1070~\rm cm^{-1}$. This is similar to carbonate peaks found in sodium borates. The same phenomenon appears in other alkali tellurite samples [Colour available online]

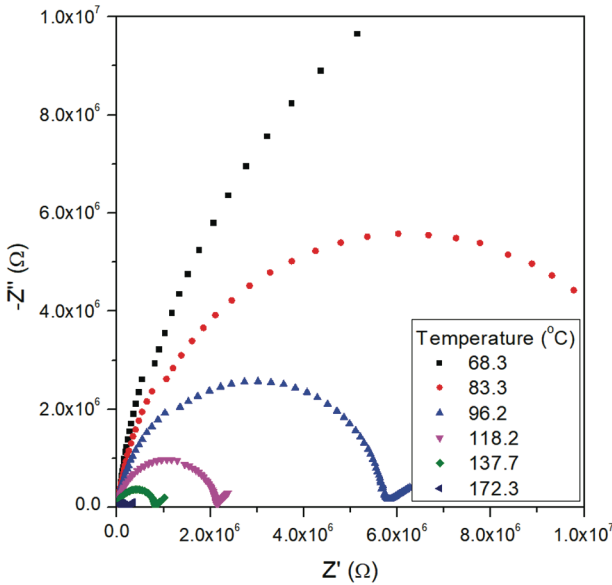


Figure 14. Nyquist plot (Opposite of the imaginary part of the impedance as a function of the real part of the impedance) for a pellet made with x = 0.65 lithium tellurite glass and measured at different temperatures [Colour available online]

good a model fits the experimental data). See Table 2 for activation energies.

For higher concentrations and for the other alkali containing tellurite glasses, the Nyquist plots exhibited two barely distinguishable half-circles, which could result from either very minor phase separation or more likely the existence of a grain boundary resistance just barely significant enough to be detected by the EIS instrument. The existence of a second phase creates challenges for the interpretation of the data, and small errors may arise as a consequence. Therefore, in this work, we only present the results found for single-phase analysis.

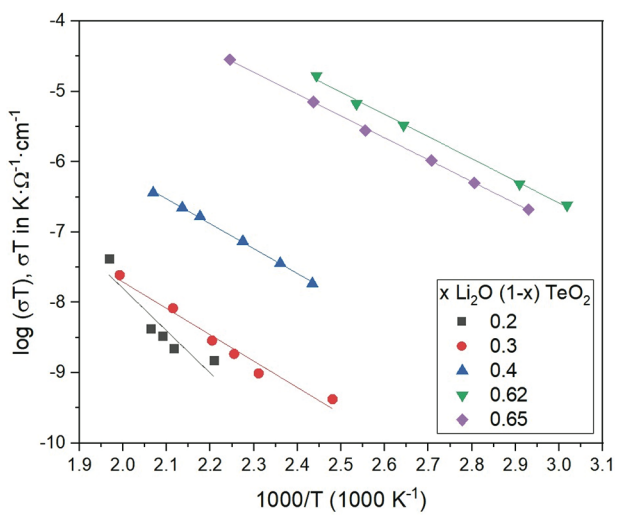


Figure 15. Arrhenius plot of the ionic conductivity of the lithium tellurite glass samples. The slope is proportional to the activation energy (E_A) of the process, and the E_A s are reported in Table 2 [Colour available online]

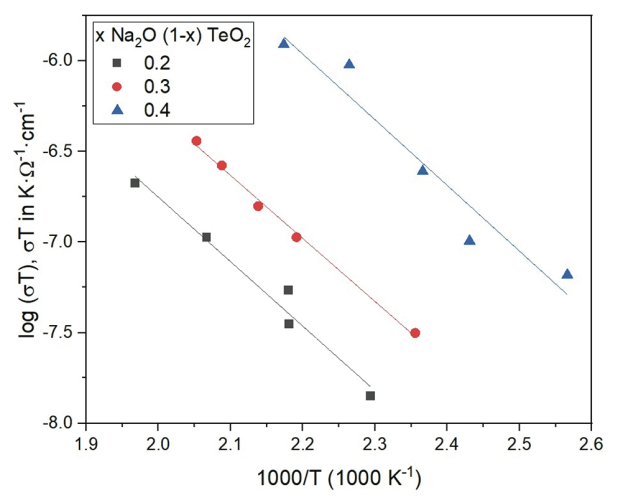


Figure 16. Arrhenius plot of the ionic conductivity of the sodium tellurite glass samples. The slope is proportional to the activation energy (E_A) of the process, and E_A s are reported in Table 2 [Colour available online]

The activation energies found in this work were plotted as a function of the composition. Results found in this work were compared to data from the literature, (22) and are illustrated in Figure 17. As it can be seen, the data are in good agreement at lower compositional ranges, and the trend found matches the data from the literature. The behaviour observed here has been found in other glasses, (16) showing an expected behaviour for the tellurite glasses. Although not presented here, it is expected that the other alkali glasses would follow a similar behaviour, given that they present a single phase.

7. Conclusion

Alkali tellurite glasses of the form $xM_2O.(1-x)TeO_2$ were made successfully over $0 \le x \le 0.80$ for lithium,

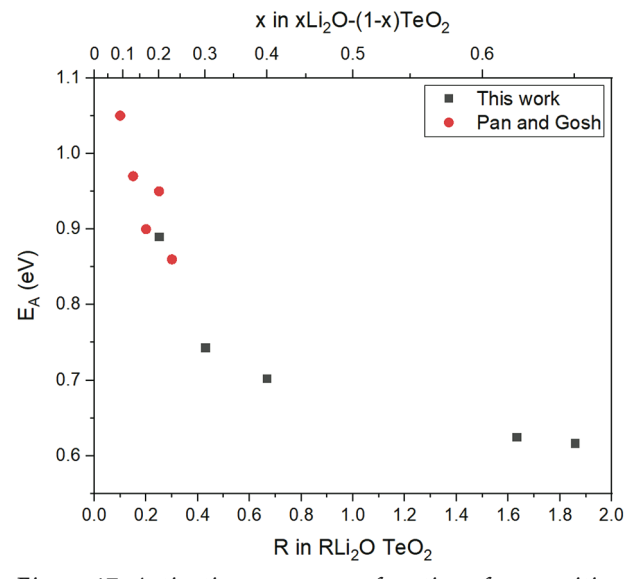


Figure 17. Activation energy as a function of composition for the lithium tellurite glasses from this work and from Pan & Gosh⁽²²⁾ [Colour available online]

YI WEI ET AL: EXTENDING THE GLASS FORMATION OF ALKALI TELLURITES

 $0 \le x \le 0.65$ for sodium, $0 \le x \le 0.35$ for potassium, and $0 \le x \le 0.35$, $0 \le x \le 0.25$ for rubidium and cesium. Here x is the molar fraction of alkali carbonate used in the batch. For the lithium and sodium cases, the new results significantly extended the known ranges of glass formation. For higher alkali contents, the thermal stability of these glasses were low resulting in rapid crystallisation; this necessitated the use of twin-roller quenching to form glass. The thermal properties were tested by DSC and STA. The $T_{\rm g}$ decreases in all alkali tellurite systems as alkali content increases. The T_x increases and reaches a maximum at x=0.15 or 0.20then decreases to the end of the forming range. The stability also reaches a weak maximum between x=0.15 and 0.20 for K, Rb, and Cs tellurites. The stability then decreases to near 0° C as x increases. There is a second glass-forming range for lithium tellurite glass over $0.60 \le x \le 0.80$. For sodium tellurites glass is continuously made from x=0 to 0.625.

The density of the glass was determined using a pycnometer. The density decreases as the alkali modifier content increases except for the cesium case. The molar volume and packing fraction change according to the difference in radii between modifiers and oxygen.

The Raman spectra for all glasses have three peaks that are observed within the wavenumbers peaks of 770, 660 and 460 cm⁻¹.

The carbonate retention was found by reduced weight loss of the sample and from the Raman spectra by a peak near $1050-1070 \text{ cm}^{-1}$, for x>0.50.

Ionic conductivities were obtained for lithium and some sodium tellurite glasses. The values for activation energy (E_A) were compared with others found in the literature and show a good agreement for the lower lithium concentrations and the values at higher lithium concentrations indicate a consistent lowering of the E_A trend.. Future research should include a more extensive study on the ionic conductivity of these highly modified and novel glasses.

References

- 1. Kim, S. H. Nonlinear optical properties of TeO $_2$ -based glasses: Li (Na and K) $_2$ O–TeO $_2$ binary glasses. *J. Mater. Res.*, 1999, **14** (3), 1074–83.
- Nascimento, M. L. F., & Watanabe, S. Universal curve of ionic conductivities in binary alkali tellurite glasses. *Braz. J. Phys.*, 2006, 36, 795–8.

- 3. Kavaklıoğlu, K. B., Aydin, S., Çelikbilek, M. & Ersundu, A. E. The TeO_z-Na₂O System: thermal behavior, structural properties, and phase equilibria. *Int. J. Appl. Glass Sci.*, 2015, **6** (4), 406–18.
- Sekiya, T., Mochida, N., Ohtsuka, A. & Tonokawa, M. Raman spectra of MO_{1/2}TeO₂ (M= Li, Na, K, Rb, Cs and Tl) glasses. J. Non-Cryst. Solids, 1992. 144. 128–44.
- Barney, E. R., Hannon, A. C., Holland, D., Umesaki, N. & Tatsumisago, M. Alkali environments in tellurite glasses. *J. Non-Cryst. Solids*, 2015, 414, 33–41.
- Marple, M. A., Jesuit, M., Hung, I., Gan, Z., Feller, S. & Sen, S. Structure of TeO₂ glass: results from 2D ¹²⁵Te NMR spectroscopy. *J. Non-Cryst.* Solids, 2019. 513, 183–90.
- Garaga, M. N., Werner-Zwanziger, U., Zwanziger, J. W., DeCeanne, A., Hauke, B., Bozer, K. & Feller, S. Short-range structure of TeO₂ glass. J. Phys. Chem. C, 2017, 121 (50), 28117–24.
- Himei, Y., Miura, Y., Nanba, T. & Osaka, A. X-ray photoelectron spectroscopy of alkali tellurite glasses. J. Non-Cryst. Solids, 1997, 211 (1–2), 64–71.
- Alderman, O. L. G., Benmore, C. J., Feller, S., Kamitsos, E. I., Simandiras, E. D., Liakos, D. G., Jesuit, M., Boyd, M., Packard, M. & Weber, R. Short-Range Disorder in TeO₂ Melt and Glass. *J. Phys. Chem. Lett.*, 2019. 11 (2), 427–31.
- Tagiara, N. S., Palles, D., Simandiras, E. D., Psycharis, V., Kyritsis, A. & Kamitsos, E. I. Synthesis, thermal and structural properties of pure teo₂ glass and zinc-tellurite glasses. *J. Non-Cryst. Solids*, 2017, 457, 116–25.
- Hauke, B., Barney, E. R., Pakhomenko, E., Jesuit, M., Packard, M., Crego, A., Tarantino, G., Affatigato, M. & Feller, S. Structure and Glass Transition Temperatures of Tellurite Glasses. *Phys. Chem. Glasses: Eur. J. Glass Sci. Technol. B*, 2020, 61 (1), 21–6.
- Kamitsos, E. I., Karakassides, M. A. & Patsis, A. P. Spectroscopic study of carbonate retention in high-basicity borate glasses. *J. Non-Cryst. Solids*, 1989, 111 (2–3), 252–62.
- Reference Tables. NIST Center for Neutron Research. 2017, https:// www.nist.gov/ncnr/sample-environment/sample-mounting/reference-tables
- Shannon, R. D. Revised effective ionic radii and systematic studies of interatomic distances in halides and chalcogenides. *Acta Crystallogr.* A, 1976, 32 (5), 751–67.
- Giri, S., Gaebler, C., Helmus, J., Affatigato, M., Feller, S. & Kodama, M. A General study of packing in oxide glass systems containing alkali. J. Non-Cryst. Solids, 2004, 347 (1–3), 87–92.
- Ruckman, A., Beckler, G., Guthrie, W., Jesuit, M., Boyd, M., Slagle, I., Wilson, R., Barrow, N., Tagiara, N. S., Kamitsos, E. I., Feller, S. & Bragatto, C. B. Lithium ion sites and their contribution to the ionic conductivity of RLi₂O-B₂O₃ glasses with R≤ 1·85. Solid State Ionics, 2021, 359, 115530.
- Impedance Spectroscopy: Theory, Experiment, and Applications. Edited by E. Barsoukov & J. R. Macdonald, John Wiley & Sons, 2018
- Dimitrov, V. & Komatsu, T. Correlation Among electronegativity, cation polarizability, optical basicity and single bond strength of simple oxides. J. Solid State Chem., 2012, 196, 574–8.
- Tagiara, N. S. Synthesis, structure and properties of pure TeO₂ glass, binary and ternary tellurite glasses. PhD Thesis, University of Athens, 2022.
- Papadopoulos, A. G., Tagiara, N. S., Simandiras, E. D. & Kamitsos, E. I. On the absence of doubly bonded Te–O groups in TeO₂ glass. *J. Phys. Chem. B*, 2020, **124** (27), 5746–53.
- Zhang, H., Koritala, S., Farooqui, K., Boekenhauer, R., Bain, D. & Kambeyanda, S. A Model for carbon dioxide retention in alkali borate and borosilicate systems. *Phys. Chem. Glasses*. 1991, 32 (5), 185–7.
- Pan, A. & Ghosh, A. Ionic conductivity and relaxation dynamics in lithium tellurite glasses. *Phys. Rev. B*, 1999, 60 (5), 3224.